

<https://doi.org/10.15407/knit2024.06.020>
UDC 629.765

V. A. PROROKA¹, PhD student
<https://orcid.org/0000-0001-6884-3934>
E-mail: v.proroka@gmail.com

S. V. ALEKSEYENKO², Prof., Doctor of Technical Sciences
<https://orcid.org/0000-0003-0320-989X>
E-mail: aleksieienko.s.v@nmu.one

¹Dnipro National University named after Oles Honchar
72, Gagarin Ave., Dnipro, 49010 Ukraine

²National Technical University “Dnipro Polytechnic”
19 Dmytro Yavornytsky Ave., Dnipro, Ukraine

AERODYNAMIC CALCULATION OF THE ULTRALIGHT SUBORBITAL ROCKET K110 SU

Calculation of aerodynamic characteristics of aircraft is an important stage in solving the tasks of their design and refinement. Aerodynamic computations are required to determine the optimal aerodynamic shape, conduct ballistic computations, develop the control system, strength calculations, and solutions for other tasks arising in the design of aircraft. In this study, the aerodynamic characteristics of suborbital rocket K110 SU were analyzed using the method of three-dimensional Navier-Stokes equations averaged according to Reynolds. For closing up the system of equations, the SST $k-\omega$ model of turbulence was chosen. A numerical solution of the Navier-Stokes equation was obtained with the help of the control volume method. In calculations, the method of the 2nd order of approximation in spatial variables was used. Verification of this method was done by comparison of the obtained computational results with known experimental data. For the developed structural and compositional layout of the rocket, the dependence of the frontal drag on the Mach number and roughness of the surface was investigated. Peculiarities of the structure of the flow with consideration of the shape of the fairing and aerospike were determined, and their influence on the aerodynamics of the vehicle was analyzed. Dependences of aerodynamic properties on the velocity of flight at subsonic, transonic, and supersonic modes of the airflow were obtained. Based on the obtained results, recommendations for the choice of geometric parameters of ultralight suborbital rockets were developed from the point of view of minimization of the head drag factor during the flight on a given trajectory within the determined range of Mach numbers. The obtained results can be used in designing new and improving existing samples of ultralight suborbital rockets.

Keywords: aerodynamics, computational fluid dynamics, numeric methods, aerodynamic coefficients, suborbital rocket.

Introduction. Calculation of the aerodynamic characteristics of flying vehicles is an important stage in the process of their design and refinement. Aerodynamic computations are necessary for determining the optimal aerodynamic shape of the rocket, carrying out ballistic computations, the development of

the control system, strength calculations, and solving other tasks arising in the design of flying vehicles. Besides, each rocket has its peculiarities and moves on its own flight trajectory and, therefore, requires its own aerodynamic computations. Numerical methods based on the Navier-Stokes equations are often

Цитування: Proroka V. A., Alekseyenko S. V. Aerodynamic calculation of the ultralight suborbital rocket K110 SU. *Space Science and Technology*. 2024. **30**, No. 6 (151). P. 20–30. <https://doi.org/10.15407/knit2024.06.020>

© Publisher PH «Akadempriodyka» of the NAS of Ukraine, 2024. This is an open access article under the CC BY-NC-ND license (<https://creativecommons.org/licenses/by-nc-nd/4.0/>)

used to determine aerodynamic properties, along with experimental studies in wind tunnels.

For suborbital rockets, the share of energy losses due to head aerodynamic drag is higher compared to conventional launch vehicles. This is because traditional launch vehicles have a much larger liftoff mass necessary to obtain the velocities required to reach orbits. Besides, we should note that most of the trajectory of suborbital rockets lies in the dense layers of the atmosphere.

Thus, in designing suborbital rockets, aerodynamic issues should be given special attention.

At Noosphere Space Lab Engineering School, since 2018, works on the development of a Ukrainian family of ultralight suborbital rockets have been carried out [4, 7–9]. One such project is the design of the K110 SU ultralight suborbital rocket. This rocket is designed to reach an apogee of over 10 km and will be used to test an advanced control system in the future.

The purpose of this work is to develop a method for determining the aerodynamic characteristics of suborbital rockets on the example of K110 SU.

Physical formulation of the problem. A one-stage suborbital rocket, from the aerodynamic viewpoint, is a body of revolution with large elongation. The aerodynamic flow, in which a body of revolution moves, can be considered as a sum of two flows: longitudinal and transversal. For suborbital rockets, a typical flight is one with small angles of attack; therefore, the airflow is predominantly determined by the longitudinal direction of the flow.

At a zero angle of attack, for bodies with circular cross-sections, a peculiarity of the structure of the flow around the object is the change of thickness and state of the borderline layer of the flow along the surface of the object. The thickness of the borderline layer tends to increase along the body, and its state tends to transit from laminar to turbulent.

The aerodynamic characteristics of the rocket bodies depend on their geometric parameters and the conditions and modes of the flow along them. In the process of designing the rocket bodies, it is necessary to ensure the lowest aerodynamic drag and to minimize the harmful interference with the aerodynamic stabilizers.

The drag experienced by the rocket bodies depends on a number of aerodynamic and geometric

parameters. Geometric parameters include, first of all, the outer shape of the rocket body, and the nature of processing of the surface of the streamlined body. Aerodynamic parameters include the Reynolds number Re and the Mach number M_∞ , and also the angle of attack α . Analysis of the resistance of bodies of rotation is done by separate segments — nose, central (which is usually cylindrical), and stern parts.

At small subsonic velocities, the head drag coefficient almost does not depend on M_∞ numbers and rather strongly depends on the angles of attack. With the increase of M_∞ numbers, the drag increases due to the appearance of wave resistance, which is related to the formation of local supersonic zones and compression shocks. The smoothness of the contour and increase of elongation of the nose part λ_{np} decreases depression on the larger part of its surface.

The nose part of the rocket body substantially influences the overall aerodynamic characteristics of the rocket. The simplest form of an axial-symmetric body is a combination of the nose part in the shape of a cone, an ogive, or more complicated solids of rotation with a cylindrical part behind it. In the area of the nose part and its transition into the cylinder, the most significant changes in the distribution of pressure are observed, which are influenced by the viscosity and compressibility of the gas; therefore, their consideration is of particular interest.

In turn, the drag of the nose parts strongly depends on their elongation and, at a given elongation, on their outlining shape.

One of the methods for reducing the aerodynamic drag at the nose parts of the rockets is the use of aerospikes. Aerospikes are effective predominantly in the range of supersonic speeds. Their presence shifts the location of the shockwave formed by a forward-moving flying vehicle in such a way that the shockwave does not touch the nose part of the vehicle. There are examples of the use of such structural elements on some American ballistic missiles and Soviet man-portable surface-to-air missile 9K38 Iгла.

Losses in the speed of suborbital rockets due to aerodynamic drag can be significantly influenced by the roughness parameter, which quantitatively represents the nature of the streamlining surface. To estimate the influence of roughness, equivalent equigranular roughness is used, as the actual roughness

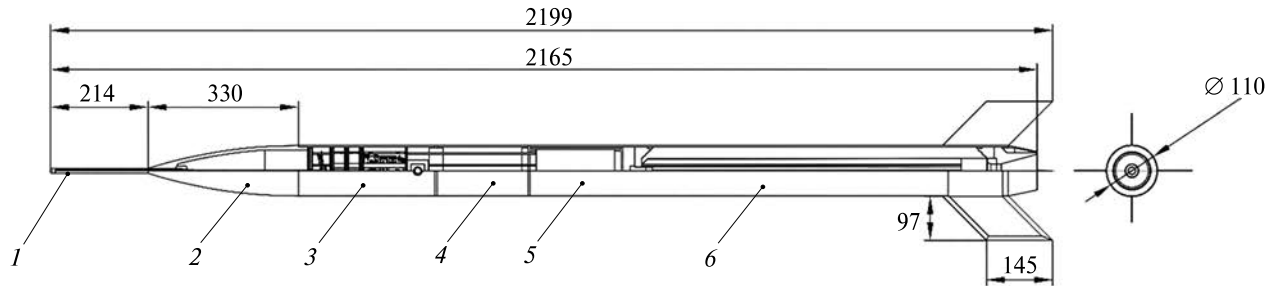


Figure 1. Design and composition diagram of the K110 SU rocket: 1 — aerospike, 2 — aerodynamic fairing, 3 — onboard electronic equipment bay, 4 — control system bay, 5 — parachute bay, 6 — solid propellant rocket motor

can vary in nature, density, and shape of irregularities. The size of the granules of roughness is chosen such that the created drag is equal to the drag created by the surface with the actual roughness.

This work considers the influence on the nature of airflow around the K110 SU ultralight suborbital rocket of such factors as:

- shape and elongation of the nose section;
- presence of the aerospike;
- roughness of the surface of the external contours of the rocket.

The geometry of the K110 SU rocket in its initial variant is shown in Figure 1. A preliminary ballistic calculation yielded the estimated flight and technical characteristics provided in Table 1.

Mathematical formulation of the problem. Calculations of the external incidence airflow were done for the subsonic, transonic, and supersonic flow with the

use of Navier-Stokes equations averaged according to Reynolds. The governing equations can be written in a three-dimensional form as [1, 3, 10]:

$$\frac{\partial \hat{p}}{\partial \hat{t}} + \nabla \cdot (\hat{\rho} \hat{U}) = 0, \quad (1)$$

$$\frac{\partial (\hat{\rho} \hat{u})}{\partial \hat{t}} + \nabla \cdot (\hat{\rho} \hat{u} \hat{U}) = -\frac{\partial \hat{p}}{\partial \hat{x}} + \nabla \cdot \hat{\tau}_x, \quad (2)$$

$$\frac{\partial (\hat{\rho} \hat{v})}{\partial \hat{t}} + \nabla \cdot (\hat{\rho} \hat{v} \hat{U}) = -\frac{\partial \hat{p}}{\partial \hat{y}} + \nabla \cdot \hat{\tau}_y, \quad (3)$$

$$\frac{\partial (\hat{\rho} \hat{w})}{\partial \hat{t}} + \nabla \cdot (\hat{\rho} \hat{w} \hat{U}) = -\frac{\partial \hat{p}}{\partial \hat{z}} + \nabla \cdot \hat{\tau}_z, \quad (4)$$

$$\frac{\partial (\hat{\rho} \hat{E})}{\partial \hat{t}} + \nabla \cdot (\hat{\rho} \hat{E} \hat{U}) = \hat{q} - \nabla \cdot (\hat{\rho} \hat{U}) + \nabla \cdot (\hat{\tau} \hat{U}), \quad (5)$$

where u, v, w are components of the vector of velocity in $x, y,$ and z directions; ρ, p are density and pressure, other designations are commonly accepted. Here, density is modeled by the state equation of ideal gas. Shear stress is modeled by Stokes' hypothesis. And viscosity is modeled by Sutherland's law. Noted the hat “ $\hat{\square}$ ” in the equations denotes that the corresponding variable has dimension, whereas symbols without the hats in this paper denote dimensionless parameters.

For closing the system of specified equations (1)–(5), the turbulence model SST $k-\omega$ was chosen. A numerical solution of the Navier-Stokes equations was obtained with the help of the control volume method. In computations, methods of the second order of approximation of spatial variables were used.

The proposed model of the computational area is a combined ellipsoid (Figure 2). The use of this geo-

Table 1. Indicative flight and technical data of the K110 SU rocket

Characteristic	Value
Apogee altitude, m	12650
Maximum velocity, m/s, (Mach)	932 (2.864)
Maximum g-force, units of g	23.27
Time to the apogee, s	43
Time of operation of the engine, s	8
Altitude at the end of the boost path, m	4410
Total mass, kg	19.136
Dry mass, kg	9.469
Diameter, m	0.11
Full length, m	2.199
Elongation, units	20

metric shape permits a reduction of the number of nodes for further building of the computational mesh. Inside the ellipsoid, the geometric model of the K110 SU suborbital rocket is placed in accordance with its above-described geometry.

An unstructured computational mesh, a structure formed by polyhedral cells, was used (Figure 3). This made it possible to reduce the total number of cells compared to the tetrahedron or hybrid meshes. The use of polyhedral cells helped to increase the accuracy of the solution and improve convergence of the computational process in comparison with the triangular mesh, which resulted in shortening the time of computation.

The computational mesh was condensed around the surface of the object in the airflow to ensure that the minimal step of the near-wall mesh satisfied the condition $y^+ < 1$, where y^+ is the dimensionless thickness of the viscous sublayer

$$y^+ = \frac{u_\tau \Delta y_1}{\nu}, \quad (6)$$

where

$$u_\tau = \sqrt{\frac{\tau_w}{\rho}}$$

— is the friction velocity,

$$\tau_w = \frac{C_f \rho U_\infty^2}{2} \quad (7)$$

is the wall shear stress,

$$C_f = \frac{0.058}{Re^{0.2}} \quad (8)$$

is the skin friction coefficient, U_∞ is the velocity of incoming flow, Δy_1 is the absolute distance from the wall, ν is the kinematic viscosity [2, 5].

Results and discussions. Verification of the chosen computing model and mesh convergence study of the solution. In this work, for evaluation of the obtained results of numerical calculations, an analysis of the mesh convergence was performed to confirm the sufficiency of the selected dimensions of the finite element mesh. The dependence of the drag coefficient on the number of elements was investigated (Figure 4). The corresponding calculations were carried out for $M_\infty = 0.8$, which matches the transonic flow mode characterized by the greatest complexity of aerodynamic processes. The results showed a percentage decrease in the value of the drag coefficient

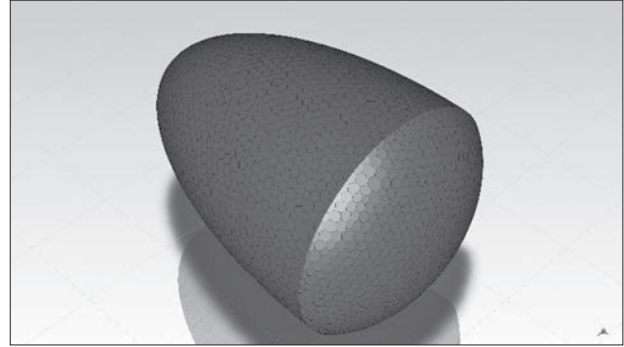


Figure 2. Spatial model of the area of calculation

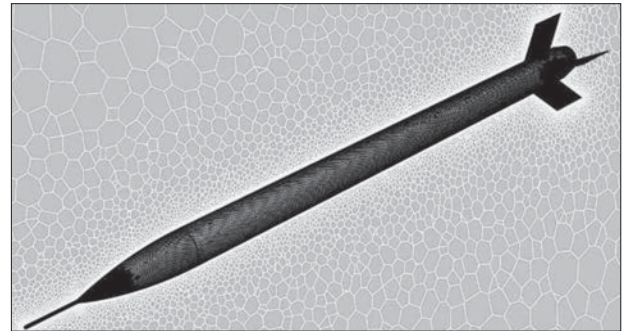


Figure 3. Computational mesh

with an increase in the number of elements of the finite element mesh. In particular, for the number of elements more than 3.5 million, a level of convergence is observed, which is expressed in the percentage deviation of the drag coefficient at the level of $\Delta C_D \leq 0.3\%$ (Figure 4, b).

To verify the chosen computational model, experimental studies were conducted on the drag coefficients of the nose parts of conical and ogive shapes (including hemisphere as a particular case of the ogive) at zero angle of attack [6]. Experiments in wind tunnels were carried out at subsonic (from $M_\infty = 0.6$) and supersonic (up to $M_\infty = 4$) speeds. The range of the Reynolds numbers was $Re = 6.65 \cdot 10^6 \dots 19.5 \cdot 10^6$. Behind the nose parts, the cylindrical part with elongation of $\lambda_{cyl} = L_{cyl} / D = 7$ was placed. Experimental data were obtained for the following elongations of conical and ogive nose parts (NP) $\lambda_{np} = L_{np} / D = [2.57, 1.54, 1.07]$ and the ogive NP in the shape of a hemisphere with elongation $\lambda_{np} = 0.5$.

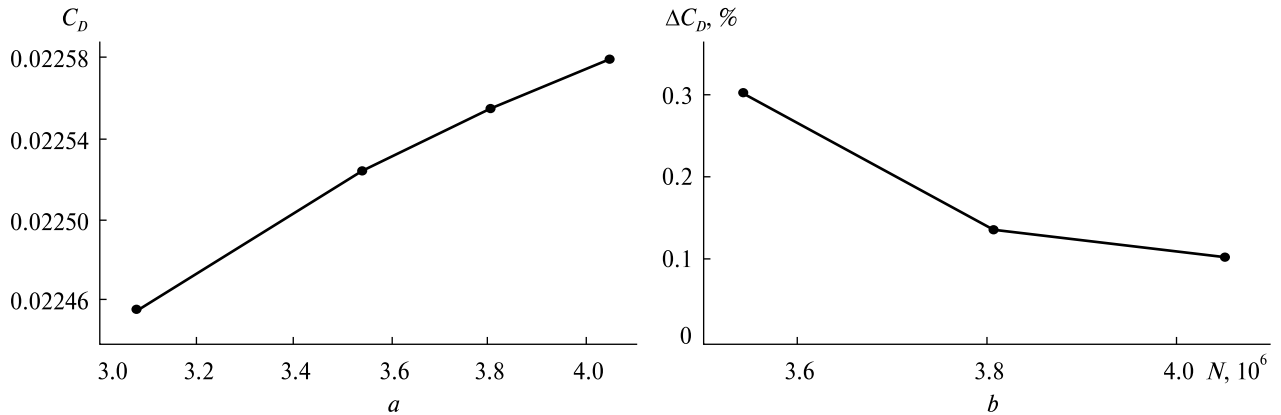


Figure 4. Evaluation of the mesh convergence depending on the number of elements of the the finite element mesh: a — $C_D = f(N)$; b — $\Delta C_D = f(N)$

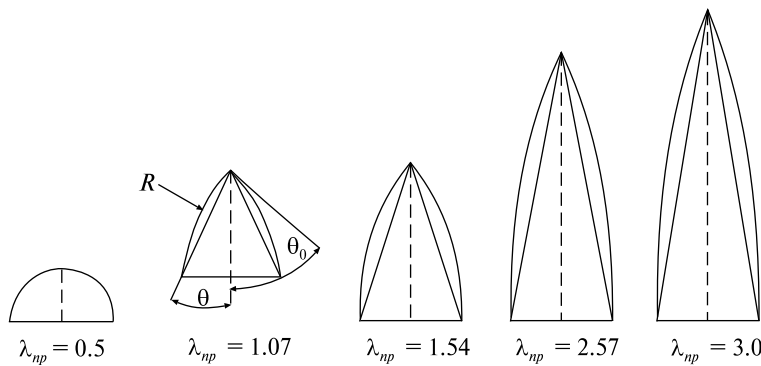


Table 2. Parameters of nose parts [8]

λ_{np}	Cone	Ogive	
	θ	θ_0	R/D
2.54	11°	22°	6.86
1.54	18°	36°	2.62
1.07	25°	49°	1.4
0.5	—	90°	0.5

Figure 5. Considered shapes of nose parts

Elongation of the NP (except the hemisphere) was chosen so that the contours of the cones were fully inscribed into corresponding ogives (Figure 5). Parameters of the nose parts are shown in Table 2.

Calculations according to the proposed computational model based on the CFD analysis preserved correspondence with the data obtained in real experiments in the Reynolds numbers criterion and geometry of the studied objects. Calculations were done in the range of Mach numbers exceeding those obtained in real experiments: $M_\infty = 0.4 \dots 5$. As a result, the dependences of the nose drag coefficient at zero angle of attack on the Mach number were obtained: $C_D = f(M_\infty)$, which were compared with the data of real experiments, as shown in Figure 6 and Figure 7.

As the obtained data demonstrate, the proposed method based on CFD analysis provides a sufficiently high level of matching the results with experimental data. The largest deviation for solids of rotation with

conical nose parts is observed in the zone of transonic velocities and does not exceed 20 %.

The value of the drag of the nose parts increases with the increase of the M_∞ number, at which the attachment of the main shockwave occurs. With a further increase of M_∞ , the drag decreases monotonically due to the rising slope of the attached shockwave and the decrease in energy loss in it. This statement is not extended to the nose part in the shape of a hemisphere, where attachment of the shockwave does not occur ($\lambda_{np} = 0.5$, Figure 7).

Given an equal elongation, the nose part of the conical shape has a sharper tip than the ogive one. Because of this, with the ogive part, attachment of the head shockwave occurs at higher values of M_∞ , causing the maximum of the dependence $c_{D0} = f(M_\infty)$ to shift to the higher values of M_∞ . The drag with the ogive nose part is lower than the conical one. This difference in drag is especially large with the nose parts

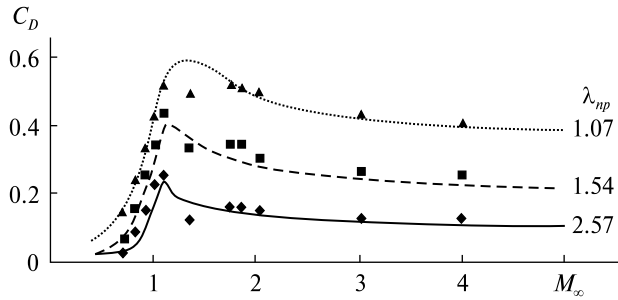


Figure 6. Dependence $C_D = f(M_\infty)$ for a conical nose part of various elongations

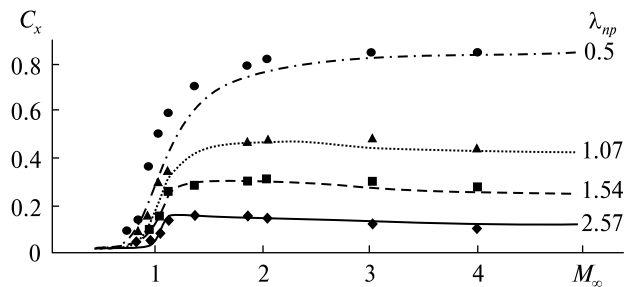


Figure 7. Dependence $C_x = f(M_\infty)$ for an ogive nose part of various elongation (2.57, 1.54, 1.07, 0.5; lines — CFD analysis, symbols — experimental data)

of small elongation in the area of transonic speeds. An explanation of a lower frontal drag of ogive nose parts can be as follows. A higher value of pressure applied at the initial area of the nose (the angle at the tip is less acute) is spread over a smaller surface area, and lower pressure applied to the rest of the ogive (with a more acute angle relative to the incidence flow than in a cone) is spread over a larger area. For M_∞ numbers, at which attachment of the head shockwave occurs, the difference of drag between conical and ogival shapes gradually reduces. This occurs because, at transonic and low supersonic speeds, the pressure at the tip is highest and gradually decreases along the rest of the contour.

Also, with the purpose of verification of the computational model, peculiarities of the structure of flow were analyzed in the combination of the conical and cylindrical parts at $M_\infty = 1.84$ (Figure 8, *a*) and the combination of the ogival and cylindrical parts at $M_\infty = 2.58$ (Figure 9, *a*). The structure of flow for the mentioned cases was compared with experimen-

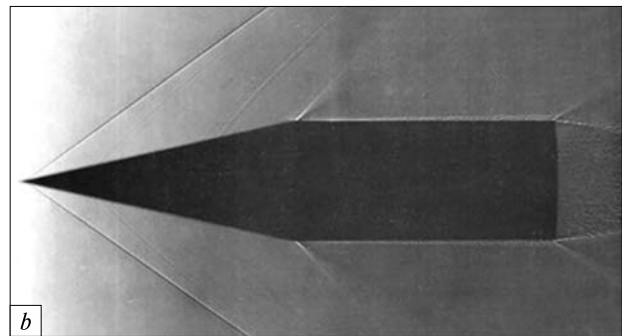
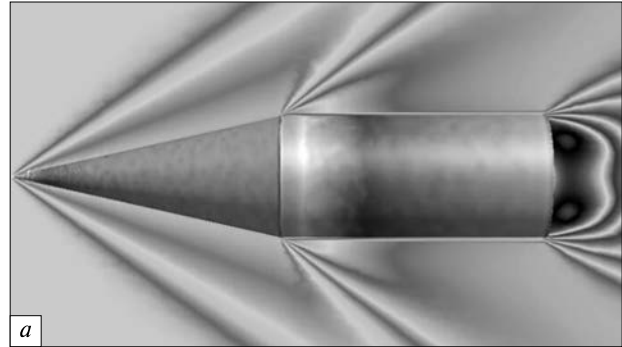


Figure 8. Structure of flow around a cone combined with a cylinder at $M_\infty = 1.84$: *a* — CFD analysis, *b* — experiment (Schlieren photography [9])

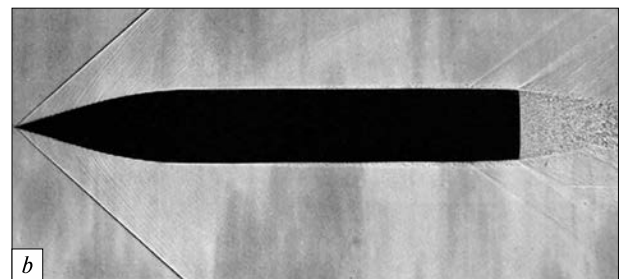
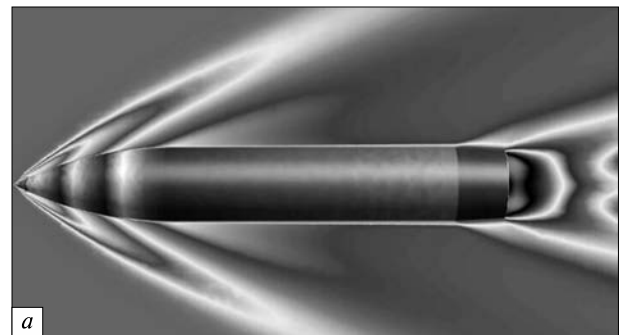


Figure 9. Flow structure around ogive-cylinder combination at $M_\infty = 2.58$: *a* — CFD analysis, *b* — experiment (Schlieren photography [9])

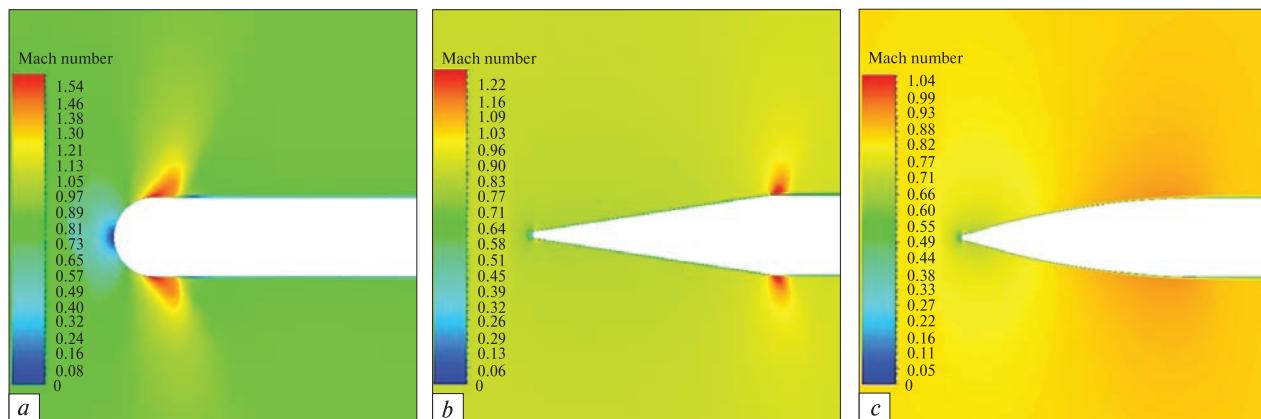


Figure 10. Formation of local supersonic zones in the flow around objects with different shapes of the nose part at $M_\infty = 0.9$: *a* — for the hemispheric NP, *b* — for a conic NP at $\lambda_{np} = 3$, *c* — for an ogival NP at $\lambda_{np} = 3$

tal data in the form of shadow images obtained with Schlieren photography [11] (Figure 8, *b* and 9, *b*, respectively). Figure 8 shows the wave structure of the formation of the compression shocks at the joining of the conic and cylindric parts. The development of a near-wall layer of a similar thickness is observed. The compression shock can be characterized as attached; the angles of the Mach cone coincide. At the bottom cross-section, a couple of oblique compression shocks form. Figure 9 shows the absence of a compression shock at the junction between the ogival and cylindrical parts. An increase in the boundary layer thickness is observed along the cylindrical part.

Influence of the shape of the nose part on the frontal drag coefficient. Since this work aims to study the aerodynamic characteristics of the K110 SU ultra-light suborbital rocket with an apogee height of about 10 km, further studies were performed for conditions

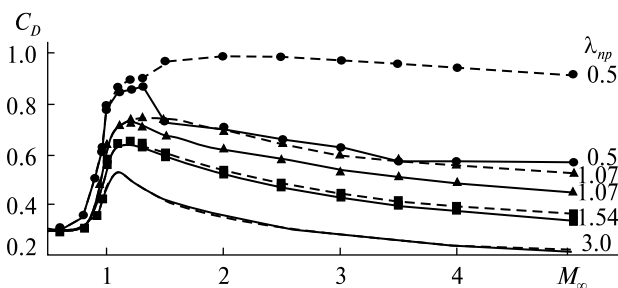


Figure 11. Dependence $C_D = f(M_\infty)$ for an ogive nose part of different elongation (3.0, 1.54, 1.07, 0.5): solid lines — with aerospike, dashed lines — without the aerospike

characterized by dense layers of the atmosphere. Let's consider images of flow around the nose part of various shapes for the K110 SU rocket.

As shown in Figures 6 and 7, a sharp increase in the frontal drag coefficient of objects with hemispheric and conic nose parts is observed at $M_\infty \approx 0.7$. At the same time, for an object with an ogival nose part of large elongation, the wave drag appears at high subsonic speeds $M_\infty \geq 0.9$. Its increase occurs less steeply in comparison with conic nose parts of similar elongation. The process of formation of supersonic areas and compression shocks forming behind them is shown in Figure 10.

In a combination of a conical nose part with a cylinder at the place of their joining, a local increase in flow speed is observed with the formation of a spike of depression. In general transonic flow modes, local supersonic speeds are achieved in these areas, creating a supersonic zone with a straight compression shock locking it. These circumstances create prerequisites for the separation of the boundary layer.

At high subsonic speeds, flow separation occurs from the ridge of the contour. At that, initially, a local supersonic zone does not form, but as the speed increases, it becomes more pronounced. With the increase in speed, the supersonic zone expands with the weakening of the closing compression shock, and the zone of separation moves down the flow. At speeds exceeding the speed of sound, supersonic flow around the object sets in, with no flow separation.

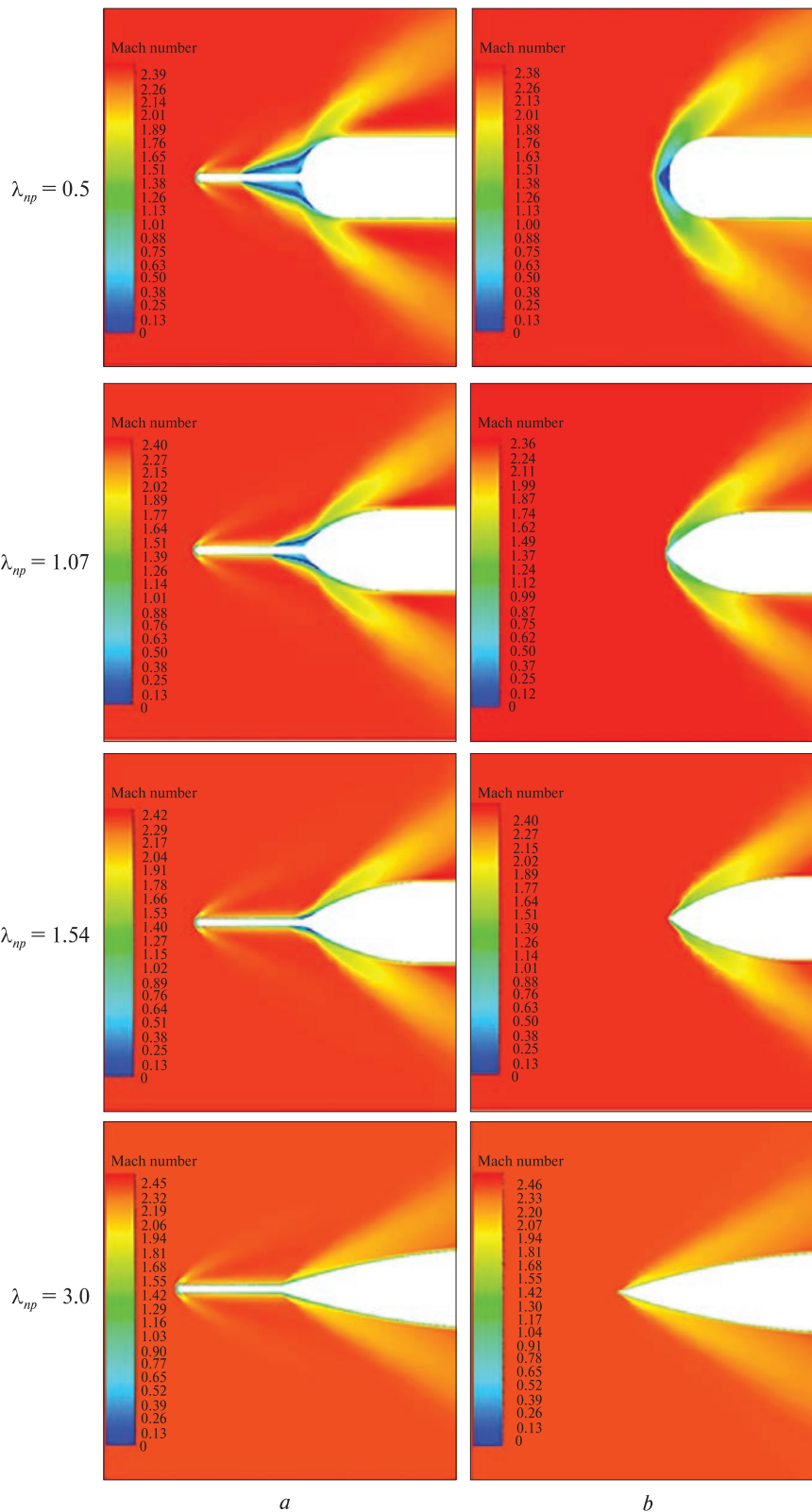


Figure 12. Image of the flow around ogive nose parts of different elongation ($\lambda_{np}=3.0$, 1.54, 1.07, 0.5): a – with aerospike, b – without the aerospike

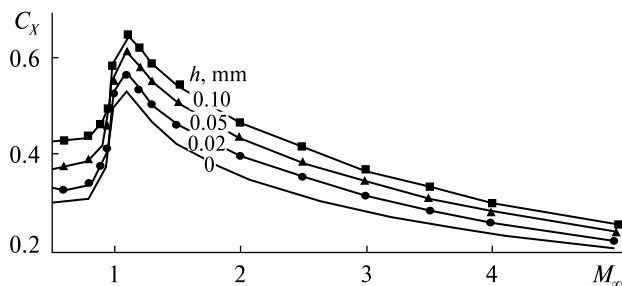


Figure 13. Dependence $C_x = f(M_\infty)$ for the K110 SU rocket with an ogive nose part for different heights of surface roughness

Behind the place of transition of the conical part into the cylinder, the pressure quickly equalizes, tending to the level of pressure in undisturbed flow. At $M_\infty \geq 2$, pressure at the rear part abruptly transits to the pressure on the cylindrical part.

The nature of pressure distribution along the object with a hemispheric nose part, just like for a combination of cone and cylinder, has a peak of low pressure at the place of joining of the nose part with the cylindrical part, with abrupt gradients at the beginning of the cylindrical part. These circumstances can also cause separation of the flow at high subsonic speeds.

In smoother nose parts with greater elongation, the nature of flow around the object changes substantially. Large pressure gradients are absent in this case, and peaks of depression reduce substantially. Therefore, for such objects, separation of the flow does not occur.

Influence of the aerospike on the frontal drag coefficient of the K110 SU rocket. For estimation of the influence of the presence of an aerospike on the head drag coefficient of the K110 SU rocket, a combination of cylindrical and ogive parts was chosen (Figure 12). The diameter of the aerospike was 11 mm, and its total length was 143 mm. On a real rocket, this aerospike is an air velocity sensor (Pitot-Prandtl tube), which can be used as the main or additional element of the control system. Ogive nose parts of different elongations were considered $\lambda_{np} = 3, 1.54, 1.07$. The obtained results are shown in Figure 11. As can be seen, the mounted aerospike shows its effectiveness, which manifests in the reduction of the frontal drag coefficient only in the zone of supersonic speeds. At $M_\infty < 1$, the presence of an aerospike re-

sults in an extremely small increase in aerodynamic drag due to the heightened friction drag from the increased surface in the flow. Analysis of Figures 11, 12 brings to a conclusion that reduction of the frontal drag coefficient occurs due to two factors: the formation of a separated shockwave at the tip of the aerospike and the development of zones of recirculation flow around the place of attachment of the aerospike to the nose part.

For ogive nose parts of small elongation, the formed recirculation zone, in which the speed of flow is much lower than M_∞ , acts as an additional component of the nose part as if it “sticks” to the solid wall. Owing to this, such a nose part represents a profile of a more streamlined shape. The reduction of effectiveness of aerospikes with the increase of elongation of ogive nose parts ($\lambda_{np} = 3.0, 2.54$, Figure 12) is because they, on their own, are bodies of more streamlined shape. This is why the formation of the zone of recirculation flow does not occur here. From this, it follows that the use of aerospikes for the reduction of the frontal drag for objects with the elongation of the nose parts $\lambda_{np} > 2.0$ is not justified. At the same time, mounting of aerospikes that can accomplish additional functions (e.g., as an airspeed sensor) practically does not change the strength of the frontal drag.

Influence of roughness of the surface on the frontal drag coefficient of the K110 SU rocket. The influence of roughness was studied for the variant of the K110 SU suborbital rocket with an ogive nose part with $\lambda_{np} = 3$ and an attached aerospike. The height of the equal-grain roughness h was varied from 0 to 0.1 mm and was set over the entire surface of the rocket except the aerospike, the surface of which was assumed to be absolutely smooth. The obtained results (Figure 13) show that the roughness factor substantially influences the magnitude of the frontal drag of a streamlined object. This influence manifests especially strongly in the zone of subsonic speeds, where the increase of the frontal drag coefficient at the height of roughness of $h = 0.1$ mm is over 30%. On the contrary, roughness’s influence on the rocket’s aerodynamic properties substantially decreases at supersonic flow with the increase of the Mach number. In general, increasing roughness nonlinearly influences frontal drag while the increment of the frontal drag reduces.

Scientific novelty. With the help of the developed method, for the K110 SU ultralight suborbital rocket, the influence of the shape of the nose part, the presence of an aerospike, and the roughness of the surface on its aerodynamic properties were studied. This makes it possible to obtain optimal combinations of these factors from the point of view of achieving the maximal altitude of the apogee and/or the mass of the payload.

Conclusions. A method of determination of aerodynamic properties of suborbital rockets based on the CFD was developed.

The proposed method was verified by comparing the calculation results with known experimental data. Deviations from the real experimental data do not exceed 20 %.

The nature of flow for nose parts of different shapes was analyzed. The lowest aerodynamic drag

is created by nose parts of an ogive shape with large elongation.

The main factors influencing the aerodynamic drag were determined, in particular, the presence of an aerospike, shape and elongation of the nose part, and roughness of the surface.

The obtained results show that the presence of an aerospike decreases aerodynamic drag for nose parts with elongation $\lambda_{np} < 2$ in the zone of supersonic speeds. For nose parts of a greater elongation, the presence of an aerospike does not practically influence the aerodynamic drag.

The roughness of the surface is a factor substantially influencing the aerodynamic properties of suborbital rockets. This influence is strongest in the zone of subsonic speeds, where the increase of the frontal drag coefficient is up to 30 %, and it reduces at supersonic speeds with the increase of the Mach number.

REFERENCES

1. Alekseyenko S., Dreus A., Dron M., Brazaluk O. (2022). Numerical Study of Aerodynamic Characteristics of a Pointed Plate of Variable Elongation in Subsonic and Supersonic Gas Flow. *J. Adv. Res. Fluid Mechanics and Thermal Sci.*, **96**(2), 88–97. <https://doi.org/10.37934/arfmts.96.2.8897>.
2. Ashgriz N., Mostaghimi J. (2002). An introduction to computational fluid dynamics. *Fluid flow handbook*, **1**, 1–49.
3. Huang D., Yang Z., Leung R. C. K. (2021). Implementation of Direct Acoustic Simulation using ANSYS Fluent. *INTER-NOISE and NOISE-CON Congress and Conf. Proc.*, **263**, No. 5, 1243–1252.
4. Kulyk O., Dron M., Solntsev V., Klymenko S., Proroka V., Yemets V. (2021). *Ways of improvement of suborbital launch vehicles*. 72nd Int. Astronaut. Congress (IAC). Technical programme, IAC-21-D2, IP, 4, x64134 (Dubai, United Arab Emirates, 25–29 October 2021).
5. Liu F. (2016). A thorough description of how wall functions are implemented in OpenFOAM. Proceedings of CFD with OpenSource software, 34. URL: https://www.tfd.chalmers.se/~hani/kurser/OS_CFD_2016/FangqingLiu/openfoamFinal.pdf (Last accessed: 18.05.2024).
6. Petrov K. P. (1998). *Aerodynamics of simplest form bodies*. M.: Factorial, 432 p. [in Russian].
7. Proroka V., Dron M., Kulyk O., Solntsev V., Abaturov A., Golubek A., Dobrodomov A. (2023). *Possibilities for expanding the application areas of suborbital launch vehicles*. 74th Int. Astronaut. Congress (IAC). Technical programme, IAC-23, D2, IP, 6, x77509 (Baku, Azerbaijan, 2–6 October 2023).
8. Proroka V., Dron M., Kulyk O., Solntsev V., Klymenko S., Dobrodomov A. (2022). *Perspectives for the use of new solutions in the creation of suborbital launch vehicles*. 73rd Int. Astronaut. Congress (IAC). Technical programme, IAC-22-D2, IP, 7, x69646 (Paris, France, 18–22 September 2022).
9. Proroka V., Dron M., Kulyk O., Solntsev V., Klymenko S. (2023). Evaluation of the results of the flight tests of the small research rocket K80 Meteo 7000 on the way to the creation of the Ukrainian family of suborbital launch vehicles. *EUREKA: Physics and Engineering*, **5**, 67–79. <https://doi.org/10.21303/2461-4262.2023.003106>.
10. Prykhodko A. A., Alekseyenko S. V., Prikhodko V. V. (2019). Numerical investigation of the influence of horn ice formation on airfoils aerodynamic performances. *Int. J. Fluid Mech. Res.*, **46**(6). <https://doi.org/10.1615/InterJFluidMechRes.2019026024>
11. VanDyke M., VanDyke M. (1982). *An album of fluid motion*. Stanford: Parabolic Press, Vol. 176.

Стаття надійшла до редакції 18.05.2024

Після доопрацювання 28.09.2024

Прийнято до друку 28.09.2024

Received 18.05.2024

Revised 28.09.2024

Accepted 28.09.2024

V. A. Пророка¹, PhD student
<https://orcid.org/0000-0001-6884-3934>
E-mail: v.proroka@gmail.com
С. В. Алексєєнко², проф., д-р техн. наук
<https://orcid.org/0000-0003-0320-989X>
E-mail: aleksieienko.s.v@nmu.one

¹ Дніпровський національний університет імені Олеся Гончара
проспект Гагаріна 72, Дніпро, Україна, 49010

² Національний технічний університет «Дніпровська політехніка»
проспект Дмитра Яворницького 19, Дніпро, Україна

АЕРОДИНАМІЧНИЙ РОЗРАХУНОК НАДЛЕГКОЇ СУБОРБІТАЛЬНОЇ РАКЕТИ К110 СУ

Розрахунок аеродинамічних характеристик літальних апаратів є важливим етапом при вирішенні завдань їхнього проектування та відпрацювання. Аеродинамічні розрахунки необхідні для визначення оптимальної аеродинамічної форми, проведення балістичних розрахунків, розробки систем керування, розрахунків на міцність та вирішення інших задач, що виникають при проектуванні літальних апаратів. У роботі дослідження аеродинамічних характеристик суборбітальної ракети надлегкого класу К110 СУ виконано на основі методики із застосуванням тривимірних усереднених за Рейнольдсом рівнянь Нав'є — Стокса. При замиканні системи рівнянь обрано модель турбулентності SST $k-\omega$. Чисельне розв'язання рівнянь Нав'є — Стокса отримано за допомогою контрольно-об'ємного методу. У розрахунках використано методи, що мають другий порядок апроксимації за просторовими змінними. Верифікацію методики виконано шляхом порівняння отриманих розрахункових результатів із відомими експериментальними даними. Для розробленої конструктивно-компонувальної схеми ракети досліджено залежність лобового опору від числа Маха та шорсткості поверхні. Визначено особливості структури течії з врахуванням форми головного обтічника та аеродинамічної голки, проаналізовано їхній вплив на аеродинаміку літального апарата. Отримано залежності аеродинамічних характеристик від швидкості польоту на дозвуковому, трансзвуковому та надзвуковому режимах обтікання. На основі отриманих результатів розроблено рекомендації щодо вибору оптимальних геометричних параметрів суборбітальної ракети надлегкого класу з точки зору мінімізації коефіцієнта лобового опору при польоті по заданій траєкторії у визначеному діапазоні чисел Маха. Отримані дані можуть бути використані при проектуванні нових та вдосконаленні наявних зразків суборбітальних ракет надлегкого класу.

Ключові слова: аеродинаміка, обчислювальна гідродинаміка, чисельні методи, аеродинамічні коефіцієнти, суборбітальна ракета.